Hindawi Publishing Corporation
Mathematical Problems in Engineering
Volume 2016, Article ID 9017481, 8 pages
http://dx.doi.org/10.1155/2016/9017481

Research Article

An Innovative Wavelet Threshold Denoising Method for Environmental Drift of Fiber Optic Gyro

Qian Zhang, Lei Wang, Pengyu Gao, and Zengjun Liu

School of Instrument Science and Opto-Electronics Engineering, Beihang University, Beijing 100191, China

Correspondence should be addressed to Lei Wang; 17wanglei@buaa.edu.cn

Received 18 September 2015; Revised 25 December 2015; Accepted 31 December 2015

Academic Editor: Francesco Soldovieri

Fiber optic gyroscope (FOG) is a core component in modern inertial technology. However, the precision and performance of FOG will be degraded by environmental drift, especially in complex temperature environment. As the modeling performance is affected by the noises in the output data of FOG, an improved wavelet threshold value based on Allan variance and Classical variance is proposed for discrete wavelet analysis to decompose the temperature drift trend item and noise items. Firstly, the relationship of Allan variance and Classical variance is introduced by analyzing the drawback of traditional wavelet threshold. Secondly, an improved threshold is put forward based on Allan variance and Classical variance which overcomes the shortcoming of traditional wavelet threshold method. Finally, the innovative threshold algorithm is experimentally evaluated on FOG. The mathematical evaluation results show that the new method can get better signal-to-noise ratio (SNR) and gain the reconstruction signal of the higher correlation coefficient (CC). As an experimental validation, the nonlinear capability of error back propagation neural network (BP neural network) is used to fit the drift trend item and find out the complex relationship between the FOG drift and temperature, and the final processing results indicate that the new denoising method can get better root of mean square error (MSE).

1. Introduction

Fiber optic gyroscope (FOG) has been widely used in inertial navigation system (INS), which was first proposed and demonstrated by Vail and Shorthill in 1976. FOG has significant advantages, such as no moving parts, short warming up time, low power consumption, impact resistance, accuracy wide coverage, and large dynamic range [1–3]. Owing to the thermal deformation itself, the drift of FOG is sensitive to environmental temperature variation and temperature related drift has become a main source of error affecting the performance of FOG in engineering application [3, 4]. At present, there are two main methods to avoid temperature drift error: one is employing machining techniques and experimental approaches to control temperature [5–8]; the other is modeling compensation method [3, 4, 9, 10]. The temperature control method has a disadvantage of increasing weight and cost, so there will be a certain amount of restraint in the application. Comparatively, the temperature modeling and compensation method is a kind of mathematical approach, which can enhance the precision of FOG by establishing an error model based on the FOG's temperature characteristics without extra hardware cost. However, during the operation of the FOG, there are a large number of random noises in the gyro signal, such as quantization noise, angle random walk, and bias instability [11]. Therefore, the temperature drift trend item is generally polluted by noises and it affects the modeling compensation accuracy.

Generally, FOG drift compensation technology includes denoising and modeling, and the denoising accuracy would influence the result of modeling. So denoising is an important step of FOG drift compensation. Wavelet analysis has achieved good effort in stochastic signal processing field because of its good time-frequency analysis ability. Many algorithms have been presented, such as wavelet transform [3, 4], wavelet packet transform [12], lifting wavelet transform [3], and wavelet threshold denoising method [13]. Among these methods, the wavelet threshold denoising method has been widely used in various situations [13, 14]. The principle of the wavelet threshold denoising method is processing

the wavelet coefficients by choosing proper threshold and threshold function [15, 16]. The methods of hard threshold and soft threshold are defined as (1) and (2), respectively:

$$\widehat{w}_{j,k} = \begin{cases} w_{j,k} & \left|w_{j,k}\right| \geq \lambda \\ 0 & \left|w_{j,k}\right| < \lambda \end{cases} \tag{1}$$

$$\widehat{w}_{j,k} = \begin{cases} \operatorname{sign}\left(w_{j,k}\right)\left(\left|w_{j,k}\right| - \lambda\right) & \left|w_{j,k}\right| \geq \lambda \\ 0 & \left|w_{j,k}\right| < \lambda, \end{cases} \tag{2}$$

where λ is the threshold value, which is defined as $\lambda = \sigma\sqrt{2\lg(N)}$. N is the length of signal, and σ is the noises standard deviation. $w_{j,k}$ represents wavelet coefficients, and $\widehat{w}_{j,k}$ represents quantized wavelet coefficients.

The traditional wavelet threshold denoising method is to process wavelet coefficients term by term. Soft threshold denoising produces constant deviation in denoising, so it would cause edge distortion; hard threshold denoising process causes additional concussion and phenomenon of disguised Gibbs. All in all, during the traditional wavelet threshold denoising processing, the noise is generally regarded as an independent sequence and meets the distribution of Gaussian white noise, which means that the traditional threshold is actually the dividing line between Gaussian white noise and other signals. In this way, the denoised signal is not the temperature drift trend item, which will directly affect the modeling performance.

To overcome this disadvantage, an improved threshold value based on Allan variance and Classical variance is proposed to extract the temperature drift trend item from original signal of FOG. The basic idea of this method is that the improved threshold is selected as the dividing line between the temperature trend item and other noise signals, thus avoiding the phenomenon of wavelet coefficients of the "overkill" and "overreservation." The experimental FOG signal is processed by the improved threshold and the results show that the proposed method effectively avoids the deficiency above. Finally, the error back propagation neural network (BP neural network) is proposed to establish the temperature drift model for compensation to demonstrate that the denoised signal with the improved method achieves better experimental performance for modeling. The training results of BP neural network show that the denoised signal with the improved method could speed up the neural network training and make the neural network reach smaller mean squared error (MSE).

2. The Relationship between Noises and Variance

The drift of FOG has a multicomponent structure and these components have different statistical characteristics [17]. Thus, there is a problem of FOG drift components statistical parameters determination to characterize gyro accuracy. Allan variance method is a time analysis technique, which is developed by Dr. David Allan, to study the characteristic of random noise terms and stability in precision oscillators used in clock application [18]. Allan variance method can be used to determine the characteristics of the underlying random processes which give rise to the data noises. Allan variance is also generally used to identify the errors of inertial sensors (i.e., gyroscopes and accelerometers) [19].

The calculation of Allan variance is based on the method of cluster analysis [19–21]. Assuming that the signal of FOG is acquired at a sampling period τ_0, separating the N sampling data into K clusters, each cluster includes m sampling data:

$$\underbrace{\omega_1, \omega_2, \ldots, \omega_m}_{k=1}, \ldots, \underbrace{\omega_{N-m+1}, \omega_{N-m+2}, \ldots, \omega_N}_{k=K}. \tag{3}$$

The relevant time is defined as $\tau = m\tau_0$. The typical Allan variance can be expressed as

$$\begin{aligned} \sigma_A^2(\tau) &= \frac{1}{2}\left\langle\left(\overline{\Omega}_{k+1} - \overline{\Omega}_k\right)^2\right\rangle \\ &= \frac{1}{2(K-1)}\sum_{k=1}^{K-1}\left(\overline{\Omega}_{k+1} - \overline{\Omega}_k\right)^2 \quad k = 1, 2 \ldots, K, \end{aligned} \tag{4}$$

where $\overline{\Omega}_k = (1/m)\sum_{i=1}^{m}\omega_{(k-1)m+i}$ represents the average value of each cluster. By varying the number of samples per cluster, variances are computed at different cluster length by (4). The relationship between Allan variance $\sigma_A^2(\tau)$ and power spectrum density (PSD) of the intrinsic random process is given by

$$\sigma_A^2(\tau) = 4\int_0^\infty S_X(f)\frac{\sin^4(\pi f\tau)}{(\pi f\tau)^2}\mathrm{d}f, \tag{5}$$

where $S_X(f)$ is the PSD of specified noise $x(t)$ and τ is the relevant time. Equation (5) indicates that the Allan variance is proportional to the total power output of the random process when passed through a filter with the transfer function of the form $\sin^4(x)/(x)^2$. This particular transfer function is the result of the method used to create and operate on the clusters [22].

The Classical variance is generally defined as (6) in time-domain:

$$\sigma_C^2 = \frac{1}{K-1}\sum_{i=1}^{K}\left(x_i - \overline{x}\right)^2, \tag{6}$$

where $\overline{x} = (1/K)\sum_{i=1}^{K}x_i$ is the average value of x_i. Actually, time-domain and frequency-domain parameters naturally are not independent. The Classical variance could be theoretically deduced from the PSD by an integral relationship. The Classical variance is defined in frequency-domain as [23]

$$\sigma_C^2(\tau) = 2\int_0^\infty S_X(f)\,\mathrm{d}f. \tag{7}$$

However (7) is defined in the context of $\tau = 0$, which is suitable for continuous-time signal. So signal $x(t)$ should be averaged and (7) can be converted into the form similar to (5):

$$\sigma_C^2(\tau) = 2\int_0^\infty S_X(f)\frac{\sin^2(\pi f\tau)}{(\pi f\tau)^2}\mathrm{d}f. \tag{8}$$

Allan variance method could be used to analyze the common five basic gyro noise terms and they are expressed in a notation appropriate for gyro data reduction [11]. The five basic noise terms are angle random walk, rate random walk, bias instability, quantization noise, and rate ramp. Each noise term could be accessed through the PSD associated with Allan variance [11, 22–24]. What is more, the relationships between Classical variance and the five noise terms are also discussed in the same way as follows.

2.1. Quantization Noise (QN). Quantization noise is strictly due to the digital nature of the FOG output. Quantization noise represents the minimum resolution of the FOG, and its PSD could be expressed as $S_X(f) = \tau_0 Q_v^2 (2\pi f)^2$. Considering (5) and (8), the Allan variance and the Classical variance of quantization noise are calculated separately as

$$\begin{aligned} \sigma^2_{A\text{-QN}}(\tau) &= \frac{3 \cdot Q_v^2}{\tau^2}, \\ \sigma^2_{C\text{-QN}}(\tau) &= \frac{2 \cdot Q_v^2}{\tau^2}, \end{aligned} \tag{9}$$

where Q_v is the quantization noise coefficient.

2.2. Angle Random Walk (ARW). The main source for this error is spontaneous emission of photons present in the FOG output. Some high-frequency noises whose relevant times are much shorter than sample time τ_0 also contribute to angle random walk. The PSD of angle random walk could be expressed as $S_X(f) = N_v^2$; then the Allan variance and the Classical variance can be expressed as

$$\begin{aligned} \sigma^2_{A\text{-ARW}}(\tau) &= \frac{N_v^2}{\tau}, \\ \sigma^2_{C\text{-ARW}}(\tau) &= \frac{2N_v^2}{\tau}, \end{aligned} \tag{10}$$

where N_v is the angle random walk coefficient.

2.3. Bias Instability (BI). The origin of this noise is the electronics or other components susceptible to random flickering. The PSD associated with this noise is $S_X(f) = B_v^2/2\pi f$. Then the Allan variance of bias instability is calculated as

$$\sigma^2_{A\text{-BI}}(\tau) = \frac{B_v^2 \cdot 2\ln 2}{\pi}, \tag{11}$$

where B_v is the bias instability coefficient. The Classical variance of rate random walk could be expressed as

$$\sigma^2_{C\text{-BI}}(\tau) = \frac{B_v^2}{\pi} \int_0^\infty \frac{\sin^2(\pi f\tau)}{(\pi f\tau)^3} \mathrm{d}(\pi f\tau). \tag{12}$$

It is clear that the integrand $\sin^2(\pi f\tau)/(\pi f\tau)^3$ is nonintegrable at lower limit of integral. However, in practice, the sampling data are discrete and limited, which means that the frequency f in (12) is limited as well. If the length of sampling data is N and the sampling frequency is f_s, the frequency f varies from f_s/N to $+\infty$ actually. Then $\sigma^2_{C\text{-BI}}(\tau)$ can be expressed as

$$\sigma^2_{C\text{-BI}}(\tau) = \frac{B^2}{\pi} \int_{(m/N)\pi}^\infty \frac{\sin^2(x)}{x^3} \mathrm{d}x, \quad m = \frac{\tau}{\tau_0}. \tag{13}$$

2.4. Rate Random Walk (RRW). Rate random walk is a random process of uncertain origin and possibly a limiting case of an exponentially correlated time. The PSD associated with this noise is $S_X(f) = K_v^2/(2\pi f)^2$. The Allan variance is

$$\sigma^2_{A\text{-RRW}}(\tau) = \frac{K_v^2 \cdot \tau}{3}, \tag{14}$$

where K_v is the rate random walk coefficient. The Classical variance of rate random walk could be expressed as

$$\sigma^2_{C\text{-RRW}}(\tau) = \frac{K_v^2 \cdot \tau}{2\pi} \int_0^\infty \frac{\sin^2(\pi f\tau)}{(\pi f\tau)^4} \mathrm{d}(\pi f\tau). \tag{15}$$

Equation (15) can be analyzed using the same method as (12). Then $\sigma^2_{C\text{-RRW}}(\tau)$ can be expressed as

$$\sigma^2_{C\text{-RRW}}(\tau) = \frac{K^2 \cdot \tau}{2\pi} \int_{(m/N)\pi}^\infty \frac{\sin^2(x)}{x^4} \mathrm{d}x, \quad m = \frac{\tau}{\tau_0}. \tag{16}$$

2.5. Drift Rate Ramp (DRR). This error is more deterministic in nature than random errors and indicates a very slow monotonic change of the FOG source of the intensity persisting over a long period of time. Generally, the changing of environmental temperature is the main origin of this error. The drift rate ramp appears as a genuine input to FOG given by $X = R_v t$, so the Allan variance of this process is

$$\sigma^2_{A\text{-DRR}}(\tau) = \frac{R_v^2 \cdot \tau^2}{2}, \tag{17}$$

where R_v is the drift rate ramp coefficient.

According to the definition of (6), the Classical variance of drift rate ramp can be expressed as

$$\sigma^2_{C\text{-DRR}}(\tau) = \frac{R^2 \cdot \tau^2}{12}(K-1)K \approx \frac{R^2}{12}(K\tau)^2, \tag{18}$$

where the definition of K is the same as in (3). So (18) could be rewritten as

$$\sigma^2_{C\text{-DRR}}(\tau) \approx \frac{R^2}{12}(K\tau)^2 = \frac{R^2}{12}(N\tau_0)^2, \tag{19}$$

where $N\tau_0$ is total sampling time. It means that the Classical variance of drift rate ramp has no relationship with the relevant time τ.

3. Improved Threshold for Wavelet Denoising

Threshold is the key of the wavelet denoising and is the value which separates the temperature drift trend item from noises. If the threshold is chosen improperly, it would lead to "overkill" or "overreservation." Comparing the reasons which

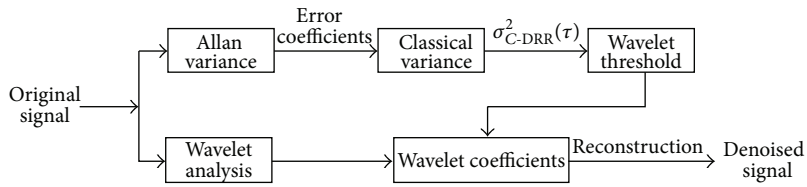

Figure 1: Scheme diagram of improved wavelet denoising algorithm.

contribute to the five errors, the drift rate ramp is the only one that related to temperature closely and the other four noise terms are not sensitive to the environment variation. Therefore, the improved threshold could be calculated according to the Classical variance $\sigma^2_C(\tau)$ in which the relevant time τ makes a distinction between $\sigma^2_{\text{C-DRR}}(\tau)$ and others.

The improved wavelet denoising algorithm is composed of five steps: Allan variance fitting, Classical variance calculation, improved threshold update, wavelet threshold denoising, and signal reconstruction. The structure of the improved wavelet denoising algorithm is shown in Figure 1.

Allan Variance Fitting Step. Generally, the coefficients of five noise terms could be identified through the Allan variance method. The theoretical analysis in Section 2 indicates that different noise terms appear in different regions of τ with different slopes, which allows easy identification of the stochastic noise terms existing in the data. According to the analysis above, the Allan variance is a sum of each type of errors and can be represented as

$$\sigma^2_A(\tau) = \sigma^2_{\text{QN}}(\tau) + \sigma^2_{\text{ARW}}(\tau) + \sigma^2_{\text{BI}}(\tau) + \sigma^2_{\text{RRW}}(\tau) + \sigma^2_{\text{DRR}}(\tau). \tag{20}$$

Fitting the log-log curve of $\sigma_A(\tau)$ versus τ with (20), the five error coefficients could be acquired from the Allan variance results.

Classical Variance Calculation Step. It is important to choose a suitable relevant time τ and then calculate the Classical variance $\sigma^2_C(\tau)$ of the five errors based on the relationship between Allan variance and Classical variance. The relevant time τ could be estimated following the principle that $\sigma^2_{\text{C-DRR}}(\tau)$ is bigger than others.

Improved Threshold Update Step. The improved threshold should be determined according to $\sigma^2_{\text{C-DRR}}(\tau)$ and it can be represented as $\lambda = \sigma_{\text{C-DRR}}\sqrt{2\lg(N)}$, where N is the length of the original signal.

Wavelet Threshold Denoising Step. Deal with the FOG signal by discrete wavelet transform and obtain the wavelet coefficients of each scale; then process wavelet coefficients with the improved threshold which has been presented in previous step.

Signal Reconstruction Step. Reconstruct the signal according to each level of the wavelet decomposition for low-frequency coefficients and high-frequency coefficients.

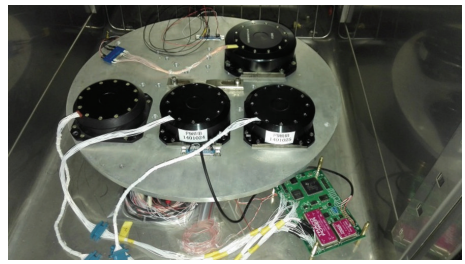

Figure 2: Test setup to collect the FOGs data.

4. Denoising Processing Results and Analysis

In order to verify the reliability of the improved threshold for wavelet denoising method, the original signal is acquired from a group of FOGs, which are fixed on an approximate horizontal stationary platform with their sensitive axes in the vertical direction as Figure 2. The temperature signal of FOG is collected by temperature sensor installed in the FOG. Multiple temperature data and FOG signals have been collected. Figure 3 shows one group of FOG signal and temperature data (angular velocity component of Earth's rotation has been subtracted).

The denoising evaluation indicators are made up of signal-to-noise ratio (SNR) and correlation coefficient (CC). When SNR is larger and CC is close to 1, the effect of denoising is better. Equations (21) and (22) represent SNR and CC, respectively:

$$\text{SNR} = 10\lg\frac{\sum_{i=1}^{N} s^2(i)}{\sum_{i=1}^{N}\left(\widehat{f}(i) - s(i)\right)^2}, \tag{21}$$

$$\text{CC} = \frac{\sum_{i=1}^{N}\left(s(i) - \overline{s}(i)\right)\left(\widehat{f}(i) - \overline{\widehat{f}}(i)\right)}{\sqrt{\sum_{i=1}^{N}\left(s(i) - \overline{s}(i)\right)^2}\sqrt{\sum_{i=1}^{N}\left(\widehat{f}(i) - \overline{\widehat{f}}(i)\right)^2}}, \tag{22}$$

where $s(i)$ is original signal and $\widehat{f}(i)$ is estimation signal after denoising. $\overline{s}(i)$ and $\overline{\widehat{f}}(i)$ are the mean value of $s(i)$ and $\widehat{f}(i)$, respectively.

Applying the Allan variance method to the whole data, a log-log plot of $\sigma_A(\tau)$ versus τ for the sampling data is shown in Figure 4. Table 1 provides each Allan analysis error coefficient of the source data.

Considering Table 1 and equations of Classical variance, the plot of $\sigma^2_C(\tau)$ versus τ is given in Figure 5. It is obvious that $\sigma^2_{\text{C-DRR}}(\tau)$ is bigger than the others after $\tau = 40$. Here, we

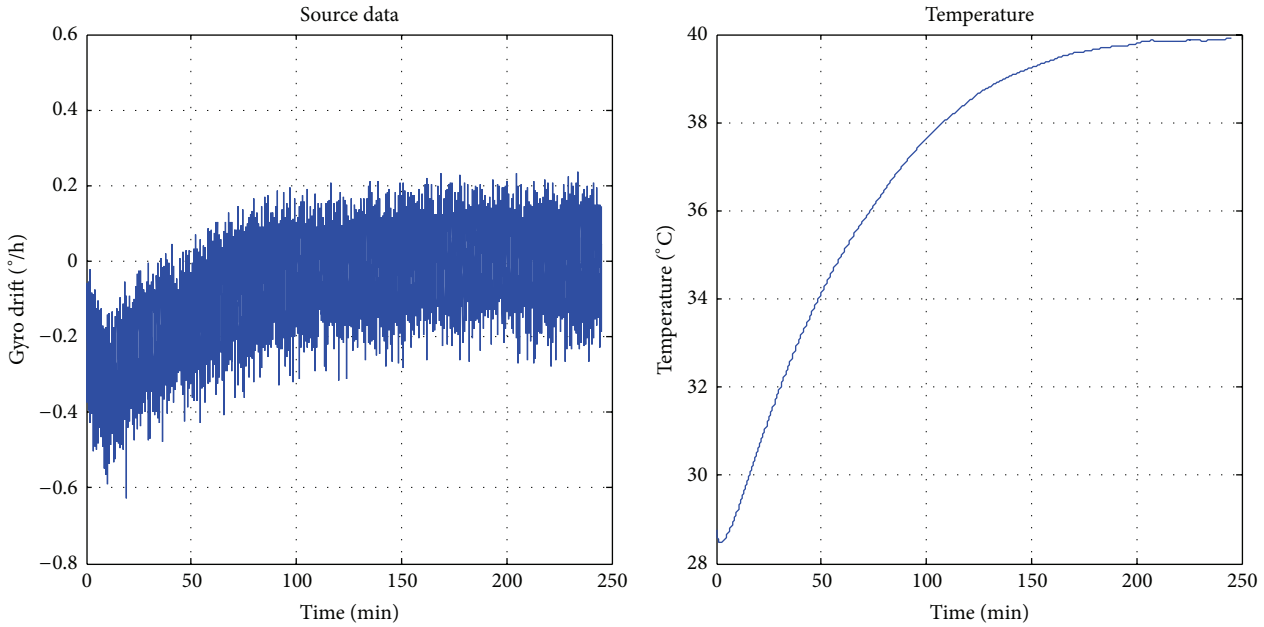

Figure 3: The measured temperature drift and temperature data of FOG.

Table 1: Fit error coefficients of Allan variance.

Error	Coefficient of error
$Q_v/(^\circ)$	0.04937
$N_v/(^\circ)\cdot h^{-1/2}$	0.04741
$B_v/(^\circ)\cdot h^{-1}$	0.008515
$K_v/(^\circ)\cdot h^{-3/2}$	0.0011697
$R_v/(^\circ)\cdot h^{-2}$	3.045e − 06

Table 2: Each Classical variance of five errors.

Classical variance/$(^\circ/h)^2$	Variance value
$\sigma^2_{\text{C-QN}}(60)$	1.354e − 06
$\sigma^2_{\text{C-ARW}}(60)$	7.492e − 05
$\sigma^2_{\text{C-BI}}(60)$	1.467e − 04
$\sigma^2_{\text{C-RRW}}(60)$	1.676e − 05
$\sigma^2_{\text{C-DRR}}(60)$	1.672e − 04

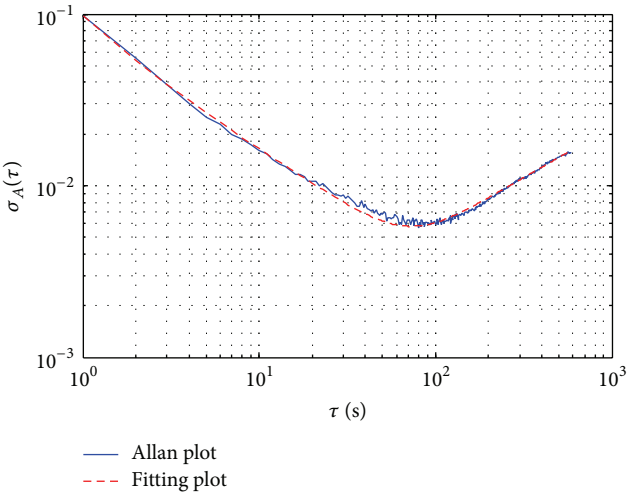

Figure 4: FOG Allan variance result.

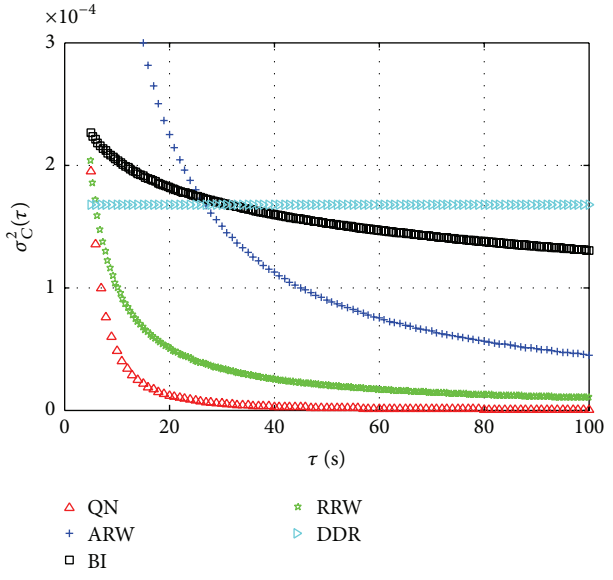

Figure 5: The Classical variance of five errors versus τ.

chose the relevant time $\tau = 60$, and the Classical variances $\sigma^2_C(60)$ are displayed in Table 2.

The improved threshold is calculated according to $\lambda = \sigma_{\text{C-DRR}}\sqrt{2\lg(N)}$, as mentioned above, and N is the length of signal. Here, $N = 14820$. The traditional threshold is chosen as the contrastive method. Figure 6 shows the results

Table 3: The Allan variance analysis results of the signal before and after denoising.

Methods	$Q_v/(^\circ)$	$N_v/(^\circ)\cdot h^{-1/2}$	$B_v/(^\circ)\cdot h^{-1}$	$K_v/(^\circ)\cdot h^{-3/2}$	$R_v/(^\circ)\cdot h^{-2}$
Original	0.04937	0.04741	0.008515	0.0011697	$3.045e-06$
Traditional threshold	0.02327	0.01892	0.005475	0.0003348	$2.982e-06$
Improved threshold	0.01029	0.01053	0.003529	0.0002952	$2.946e-06$

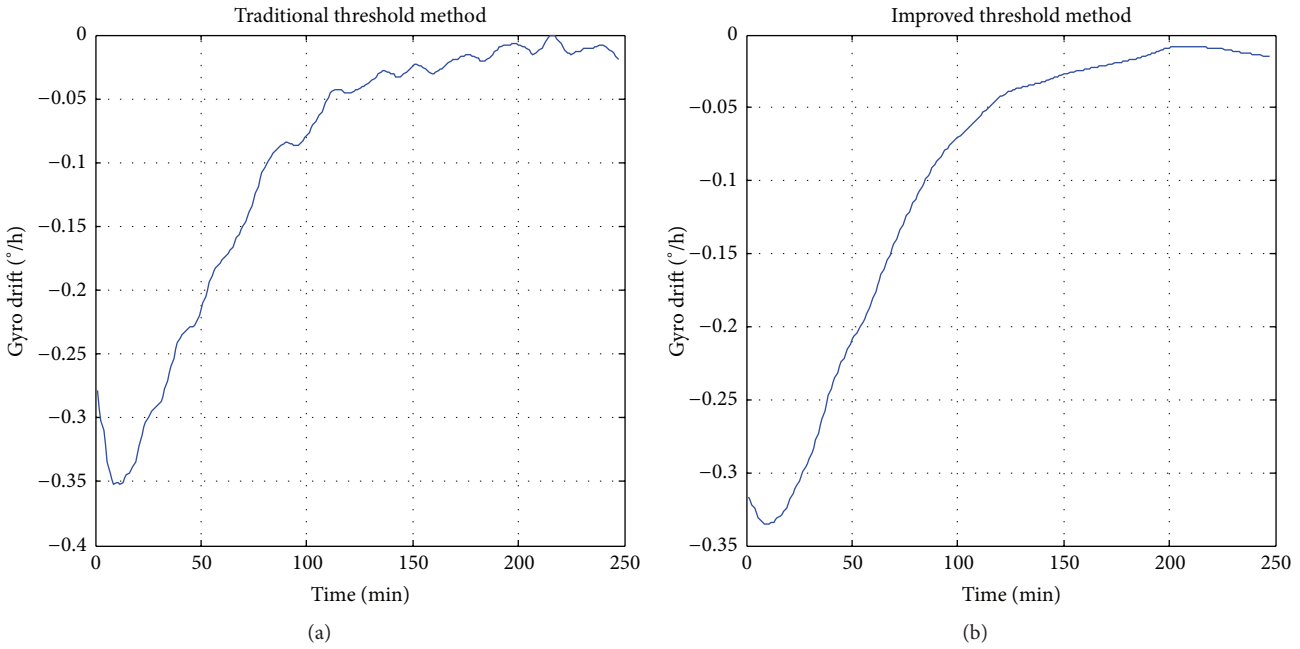

Figure 6: The results of denoising with different threshold.

of denoising with different methods. From Figure 6(a), although the drift trend item is obvious, the whole curve is not smooth, and some inflection points are superimposed on the curve. The peak-to-peak value of the fluctuations is 0.020 (°)/h approximately, which will make serious influence on the drift modeling performance. Figure 6(b) shows the result with improved threshold. It is obvious that the improved method removes noises effectively, which is good for data processing further.

Table 3 shows that each Allan analysis error coefficient of the signal denoised by improved threshold method has a significant decrease compared with the signal denoised by traditional threshold method. Moreover, the analysis results indicate that the coefficient of DRR is almost the same as original coefficient, where it is fully proved that the improved threshold is an effective method which could separate the temperature trend item and other noise signals.

Table 4 shows the results of performance evaluation with different methods. We can see that the improved threshold method gains bigger SNR and the CC of this method is more close to 1. It indicates that the effect of new denoising method is improved.

In order to demonstrate that the FOG signal denoised with the improved threshold achieves better experimental performance than traditional threshold for modeling, BP neural network is proposed to establish the temperature drift model for compensation. BP Network is a typical multilayer feed-forward neural network which has a good ability to complex nonlinear function approximation [24]. The BP Network consists of smaller units called neurons which are trained

Table 4: The denoising evaluation results.

Methods	SNR	CC
Traditional threshold	121.488	0.9877
Improved threshold	151.909	0.9902

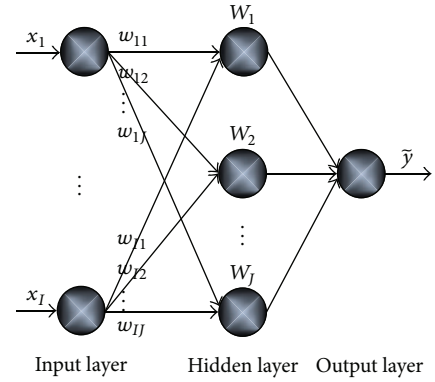

Figure 7: The model structure of BP neural network.

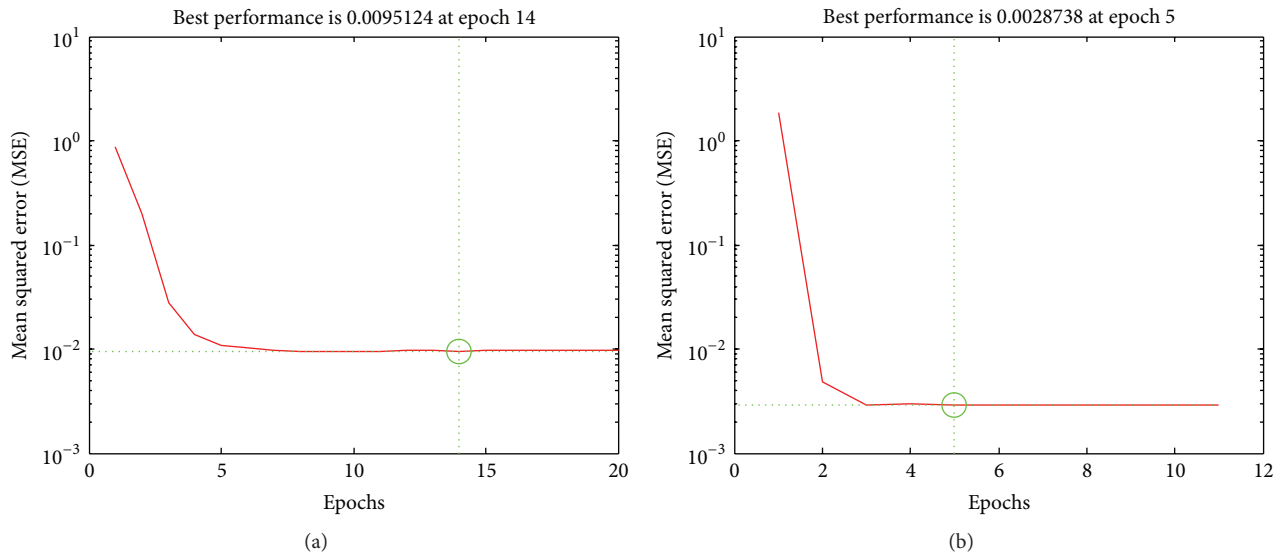

Figure 8: The comparison of mean squared error.

through a learning process, while interneuron connection strengths, known as synaptic weights, are used to store knowledge [25, 26]. As shown in Figure 7, BP Network has a simple architecture of three layers (input, hidden, and output layers). The input layer just transfers input signal to hidden layer. The hidden layer performs a fixed nonlinear transformation with no adjustable parameters and maps the input space onto a new space. The output layer then implements a linear combiner on this new space and the only adjustable parameters are the weights of this linear combiner.

The MSE comparison curves of BP neural network that is used for two groups' denoised data are depicted in Figure 8 with the same parameter of neural network. The denoised data using traditional threshold and improved threshold are named T-data and I-data, separately. Figure 8(a) is the MSE of neural network which uses the T-data, while Figure 8(b) is the MSE of neural network which uses the I-data. It is obvious that the rate of convergence in Figure 8(b) is much faster than that in Figure 8(a). The MSE in Figure 8(a) reaches its minimum value 0.0095124 at epoch 14, while the MSE in Figure 8(b) reaches its minimum value 0.0028738 at epoch 5. So the I-data could speed up the neural network training and make the neural network reach smaller MSE.

5. Conclusion

Denoising is the base of FOG environmental drift modeling and its effect would directly influence the modeling accuracy. Considering the existing shortcoming of traditional wavelet denoising method, an innovation wavelet threshold denoising method based on Allan variance and Classical variance is proposed in this paper. Among them, the improved threshold is selected based on the analysis of random noise terms of FOG signal. In this way, the improved threshold is regarded as a dividing line between the temperature trend item and other noise signals, thus avoiding the phenomenon of wavelet coefficients of the "overkill" and "overreservation." The experimental gyro signal is processed by the improved threshold and the mathematical evaluation results show that the proposed method can effectively solve the deficiency of traditional method. To demonstrate that the denoised signal with the improved method can achieve better experimental performance for modeling, BP neural network is proposed to establish the temperature drift model for compensation. The results show that the denoised signal with the improved method could speed up the neural network training and make the neural network reach smaller MSE.

Conflict of Interests

The authors declare that there is no conflict of interests regarding the publication of this paper.

References

[1] M. Narasimhappa, S. L. Sabat, R. Peesapati, and J. Nayak, "An innovation based random weighting estimation mechanism for denoising fiber optic gyro drift signal," *Optik*, vol. 125, no. 3, pp. 1192–1198, 2014.

[2] P. Lv, J. Z. Lai, J. Y. Liu, and G. Q. Qin, "Stochastic error simulation method of fiber optic gyros based on performance indicators," *Journal of the Franklin Institute*, vol. 351, no. 3, pp. 1501–1516, 2014.

[3] X. Chen and C. Shen, "Study on temperature error processing technique for fiber optic gyroscope," *Optik*, vol. 124, no. 9, pp. 784–792, 2013.

[4] G. P. Xu, W. F. Tian, Z. H. Jin, and L. Qian, "Temperature drif t modelling and compensation for a dynamically tuned gyroscope by combining WT and SVM method," *Measurement Science and Technology*, vol. 18, no. 5, pp. 1425–1432, 2007.

[5] S. Blin, H. K. Kim, M. J. F. Digonnet, and G. S. Kino, "Reduced thermal sensitivity of a fiber-optic gyroscope using an air-core photonic-bandgap fiber," *Journal of Lightwave Technology*, vol. 25, no. 3, pp. 861–865, 2007.

[6] C. X. Zhang, S. S. Du, J. Jin, and Z. G. Zhang, "Thermal analysis of the effects of thermally induced nonreciprocity in fiber optic gyroscope sensing coils," *Optik*, vol. 122, no. 1, pp. 20–23, 2011.

[7] C. M. Lofts, P. B. Ruffin, M. D. Parker, and C. C. Sung, "Investigation of the effects of temporal thermal gradients in fiber optic gyroscope sensing coils," *Optical Engineering*, vol. 34, no. 10, pp. 2856–2863, 1995.

[8] J. Sawyer, P. B. Ruffin, and C. C. Sung, "Investigation of the effects of temporal thermal gradients in fiber optic gyroscope sensing coils, part 2," *Optical Engineering*, vol. 36, no. 1, pp. 29–34, 1997.

[9] C. L. Fan, Z. H. Jin, W. F. Tian, and F. Qian, "Temperature drift modelling of fibre optic gyroscopes based on a grey radial basis function neural network," *Measurement Science and Technology*, vol. 15, no. 1, pp. 119–126, 2004.

[10] Y.-S. Zhang, Y. Y. Wang, T. Yang, R. Yin, and J. C. Fang, "Dynamic angular velocity modeling and error compensation of one-fiber fiber optic gyroscope (OFFOG) in the whole temperature range," *Measurement Science and Technology*, vol. 23, no. 2, Article ID 025101, 2012.

[11] "IEEE standard specification format guide and test procedure for single-axis interferometric fiber optic gyros," IEEE Standard 952-1997, 1998.

[12] H. M. Qian and J. C. Ma, "Research on fiber optic gyro signal de-noising based on wavelet packet soft-threshold," *Journal of Systems Engineering and Electronics*, vol. 20, no. 3, pp. 607–612, 2009.

[13] Z. R. Zhou, D. X. Huan, Y. F. Wang et al., "Improvement of the signal to noise ratio of Lidar echo signal based on wavelet denoising technique," *Optics and Lasers in Engineering*, vol. 51, no. 8, pp. 961–966, 2013.

[14] Y. Chen, L.-J. Chen, H.-L. Liu, and K. Wang, "Research on FBG sensor signal wavelength demodulation based on improved wavelet transform," *Optik*, vol. 124, no. 21, pp. 4802–4804, 2013.

[15] Y. Chen, K. Wang, H.-L. Liu, L.-J. Chen, and X. Yang, "Treatment of MZI sensor signal with an improved wavelet neighboring coefficients," *Optik*, vol. 125, no. 3, pp. 1038–1041, 2014.

[16] S. Poornachandra, "Wavelet-based denoising using subband dependent threshold for ECG signals," *Digital Signal Processing*, vol. 18, no. 1, pp. 49–55, 2008.

[17] V. V. Chikovani, "Performance parameters comparison of ring laser, coriolis vibratory and fiber-optic gyros based on Allan variance analysis," in *Proceedings of the IEEE 2nd International Conference on Actual Problems of Unmanned Air Vehicles Developments*, pp. 153–156, IEEE, Kiev, Ukraine, October 2013.

[18] H. Y. Zhao, Z. L. Wang, H. Shang, W. J. Hu, and G. Qin, "A time-controllable Allan variance method for MEMS IMU," *Industrial Robot*, vol. 40, no. 2, pp. 111–120, 2013.

[19] Q. Zhang, X. J. Niu, Q. J. Chen, H. P. Zhang, and C. Shi, "Using Allan variance to evaluate the relative accuracy on different time scales of GNSS/INS systems," *Measurement Science and Technology*, vol. 24, no. 8, Article ID 085006, 2013.

[20] L. Galleani and P. Tavella, "The dynamic allan variance," *IEEE Transactions on Ultrasonics, Ferroelectrics, and Frequency Control*, vol. 56, no. 3, pp. 450–464, 2009.

[21] L. Galleani, "The dynamic Allan variance II: a fast computational algorithm," *IEEE Transactions on Ultrasonics, Ferroelectrics, and Frequency Control*, vol. 57, no. 1, pp. 182–188, 2010.

[22] A. Makdissi, F. Vernotte, and E. De Clercq, "Stability variances: a filter approach," *IEEE Transactions on Ultrasonics, Ferroelectrics, and Frequency Control*, vol. 57, no. 5, pp. 1011–1028, 2010.

[23] S. T. Dawkins, J. J. McFerran, and A. N. Luiten, "Considerations on the measurement of the stability of oscillators with frequency counters," *IEEE Transactions on Ultrasonics, Ferroelectrics, and Frequency Control*, vol. 54, no. 5, pp. 918–925, 2007.

[24] R. Song, X. Chen, C. Shen, and H. Zhang, "Modeling FOG drift using back-propagation neural network optimized by artificial fish swarm algorithm," *Journal of Sensors*, vol. 2014, Article ID 273043, 6 pages, 2014.

[25] D. M. Song, S. C. Chen, Y. Ma, C. Shen, and Y. J. Zhang, "Impact of different saturation encoding modes on object classification using a BP wavelet neural network," *International Journal of Remote Sensing*, vol. 35, no. 23, pp. 7878–7897, 2014.

[26] F. Yu and X. Z. Xu, "A short-term load forecasting model of natural gas based on optimized genetic algorithm and improved BP neural network," *Applied Energy*, vol. 134, pp. 102–113, 2014.